

# Optimal perturbations for boundary layers subject to stream-wise pressure gradient

Peter Corbett<sup>a)</sup>

*Laboratoire de Mécanique des Fluides, École Polytechnique Fédérale de Lausanne,  
CH-1015 Lausanne, Switzerland*

Alessandro Bottaro<sup>b)</sup>

*Institut de Mécanique des Fluides de Toulouse, Université Paul Sabatier, 118 route de Narbonne,  
F-31062 Toulouse, France*

(Received 13 April 1999; accepted 30 September 1999)

Configurations of perturbation velocity which optimally excite an algebraic growth mechanism in the Falkner–Skan boundary layer are studied using a direct–adjoint technique. The largest transient amplification is obtained by stream-wise oriented vortices, in agreement with previous results for the Blasius boundary layer. Adverse pressure gradient is found to increase the resulting growth, the reverse is true for accelerated flows. It is shown that optimally excited algebraic mechanisms are capable of competition with optimally excited Tollmien–Schlichting waves in super-critical flows before succumbing to viscous damping. Disturbances optimized for maximal amplification over shorter periods are generally oblique and can experience significant transient growth; it is argued that they should not be dismissed when searching for rapidly growing perturbations which may preferentially induce early transition. Optimal disturbances transform into streaks downstream of their inception, attesting to the ubiquity of these flow structures. © 2000 American Institute of Physics. [S1070-6631(00)02101-2]

## I. INTRODUCTION

In seeking to understand the transition process, researchers have long studied the behavior of infinitesimal perturbations in model flows of physical relevance. To render the analysis tractable, such disturbances were typically presumed to be periodic and modal in nature; the ensuing system is amenable to eigenanalysis. In this context, results of such analyses reflect the behavior of the flow as it attains some asymptotic state, and historically the likelihood of transition was inferred from this state.

The study of the origin and causes of such instabilities is the field of receptivity. Here the question is how prevailing conditions at the start of a boundary layer, or environmental disturbances originating in the free-stream and present at the boundary layer's edge, will be assimilated and transformed (some distance downstream) into instabilities. One seeks to take into account the effects of such diverse excitations as small surface irregularities, acoustic forcing, and small anomalies in the oncoming mean stream due, for example, to atmospheric turbulence. Considered from the black box point of view, receptivity is the study of the “inputs,” and linearized stability theory represents the study of the “outputs.”

Work in stability theory has been recently galvanized by a growing appreciation of the importance of the “intermediate period.” Small perturbations in many flows of engineering significance might experience appreciable transient growth before assuming their asymptotic state, even if this

latter state is a stable one. Mathematically, this is due to the non-normality of the linearized operators describing the disturbances' behavior. Since the eigenvectors of such systems are nonorthogonal, constructive or destructive interference amongst the various modes is possible before modal behavior sets in.

Linear physical mechanisms for transient growth in shear layers have been described by Ellingsen and Palm,<sup>1</sup> Landahl,<sup>2</sup> and Luchini.<sup>3</sup> These mechanisms work by efficiently extracting momentum from the mean flow and transferring it to the perturbation. Twofold motivation exists for studying configurations which excite this mechanism optimally (commonly termed optimal perturbations, after Butler & Farrell<sup>4</sup>). First, is transient amplification of such magnitude that a linear model is no longer appropriate? Secondly, do these optimal perturbations resemble experimentally observed flow disturbances? In the former case, it has been hypothesized that algebraic growth may be a candidate for causing by-pass transition.<sup>5</sup>

Optimal perturbations for the algebraic growth mechanism have been extensively studied for flows of finite spatial extent, exemplified by the Couette and Poiseuille flows.<sup>4,6–8</sup> These configurations are characterized by a complete, discrete spectrum of eigenvalues which permits an arbitrary perturbation to be represented as a weighted sum of eigenvectors. The most widely used method of finding optimal perturbations for this class of flows is based on this property. The classical linear stability eigenproblem is solved, and each individual mode is assumed to evolve exponentially. Growth is then maximized using a variational approach, and the weights for the sum expressing the optimal are deter-

<sup>a)</sup>Electronic mail: Peter.Corbett@epfl.ch

<sup>b)</sup>Electronic mail: Bottaro@imft.fr

mined from the resulting generalized eigenproblem.<sup>4,6</sup> A similar variational approach is applied in an alternative method based on an initial boundary value problem formulation.<sup>7</sup> Here, the temporal behavior of a complete set of analytic basis functions must be found in order to determine the growth, and a weighted sum of these basis functions gives the optimal perturbation.

In contrast to confined flows, the spectrum of flows on a semi-infinite domain is composed of a finite number of discrete modes and a continuous spectrum.<sup>9</sup> In practical terms, this means that when the whole spectrum is determined simultaneously, using the QZ algorithm for example, a discrete numerical approximation to the continuum is obtained. However, certain numerical issues arise when using this approach: The quality of the approximation is not guaranteed, and a large number of collocation points is required to adequately resolve fine detail in the boundary layer. Since the QZ algorithm's computational cost scales as the cube of the number of points used, this approach is associated with considerable computation burden. Resolution of the continuous spectrum is a critical issue since the continuum contributes significantly to transient growth. Furthermore, as the stream-wise wave number approaches zero the discrete modes disappear completely, and it is precisely at zero wave number that the largest transient growth is found.

Butler and Farrell successfully applied the eigenvector expansion technique to the Blasius boundary layer by ingeniously considering the case of two boundary layers developing in a channel. The channel width was adjusted so as to sufficiently resolve the optimal perturbations, and the continuous spectrum was replaced by the discrete spectrum inherent to bounded flows. Their study of three-dimensional optimal perturbations in this boundary layer analog found that a stream-wise oriented vortex which evolved into a stream-wise streak provoked the most response. A similar result was found by Lasseigne *et al.*<sup>10</sup> in their extension of the initial boundary value formulation approach to boundary layers.

As mentioned in Ref. 4, an alternative technique for finding optimal perturbations can be envisioned utilizing the direct and adjoint initial boundary value problems, wherein an elegant link between the input and output states is established, and conclusions about receptivity and optimal excitations can be drawn. This approach, first suggested for tracking the growth of anomalies in weather prediction,<sup>11</sup> was used by Luchini<sup>12</sup> and Andersson *et al.*<sup>5</sup> to investigate optimals for spatially developing Blasius boundary layers. Luchini and Bottaro<sup>13</sup> applied the method in their study of the receptivity of Görtler vortices (and determined the optimal perturbation for this instability). The boundary layer scalings appropriate to these spatial analyses preclude the investigation of oblique disturbances, i.e., only phenomena asymptotically elongated in the longitudinal direction can be studied. Despite this, the results found using the spatial framework are very similar to those reported by Butler & Farrell, since they also find that stream-wise vortices excite optimal response.

The work presented here adapts the direct-adjoint technique to the temporal problem for the Falkner-Skan bound-

ary layers. In the temporal context, the parallel-flow assumption is adopted, and a uniform scaling is employed. The main advantage to this approach is that it permits the study of oblique disturbances, i.e., those flow structures whose stream-wise scale may be of comparable magnitude to their span-wise scale. Should these attain sufficient amplitude, they will enjoy a wider range of nonlinear interactions than a purely two-dimensional perturbation.<sup>14,15</sup>

Clearly, the limitation of the present study lies in the adoption of the temporal framework. Since a large number of previous studies adopt the same hypothesis, some work has focused on the identification of a transform relating the temporal transient to its spatial counterpart. In this respect, the results reported by Criminale *et al.*<sup>7</sup> and Lasseigne *et al.*<sup>10</sup> are particularly encouraging, and indicate that such a transformation may exist. Furthermore, optimal perturbations found using the temporal and the spatial techniques are in good agreement with one another, indicating that some underlying physical phenomenon is described well by either technique.

This work is devoted to the study of initial configurations which maximize the growth over a given time; these are referred to as *local* optima. The configuration which maximizes growth for all time is termed a *global* optimum. While global optima can enjoy energy growth on the order of the square of the Reynolds number, local optima also experience significant growth, and should not be discounted when exploring the different paths leading to by-pass transition. Physically, if transient growth of sufficient magnitude to induce nonlinear effects occurs in a short distance from the leading edge, the even larger growth eventually evoked further down-stream by the global optimal would be pre-empted by transition.

## II. MATHEMATICAL BACKGROUND

The behavior of a small three-dimensional velocity perturbation  $\tilde{\mathbf{u}} = (\tilde{u}, \tilde{v}, \tilde{w})^T$  in a parallel base flow,  $U = U(y)$ , is governed by the Navier-Stokes equations. Relating the stream- and span-wise perturbation velocity components to one another through the normal perturbation vorticity,  $\tilde{\eta} = (\partial\tilde{u}/\partial z) - (\partial\tilde{w}/\partial x)$ , linearizing the Navier-Stokes equations, and eliminating the perturbation pressure yields a system in  $\tilde{\mathbf{v}}$  and  $\tilde{\eta}$ <sup>16</sup>

$$\left[ \left( \frac{\partial}{\partial t} + U \frac{\partial}{\partial x} - \frac{1}{R} \Delta \right) \Delta - \frac{\partial^2 U}{\partial y^2} \frac{\partial}{\partial x} \right] \tilde{\mathbf{v}} = 0, \quad (1)$$

$$\left( \frac{\partial}{\partial t} + U \frac{\partial}{\partial x} - \frac{1}{R} \Delta \right) \tilde{\eta} = - \frac{\partial U}{\partial y} \frac{\partial}{\partial z} \tilde{\mathbf{v}}.$$

The Laplacian operator is represented above by  $\Delta = (\partial^2/\partial x^2) + (\partial^2/\partial y^2) + (\partial^2/\partial z^2)$ . At solid walls and in the free-stream the normal perturbation velocity and its normal derivative are assumed to vanish. Similarly, since the stream- and span-wise perturbation velocities vanish at these boundaries, the normal disturbance vorticity must, too. Semi-infinite domains are usually represented in a truncated com-

putational space, in which case these conditions are commonly replaced by their asymptotic equivalents at its upper limit.

The Reynolds number, which characterizes the relative importance of convective to diffusive processes

$$R = \frac{U_\infty \delta}{\nu},$$

appears when the original system is uniformly nondimensionalized using a characteristic length ( $\delta$ ) and velocity ( $U_\infty$ ). Pressure is scaled by the grouping  $\rho U_\infty^2$ . This work uses Falkner–Skan boundary layer profiles to specify  $U(y)$ , and  $\delta$  is taken to be proportional to the boundary layer thickness defined by  $\delta = \sqrt{\nu l / U_\infty}$ , with  $l$  a reference stream-wise distance.

Assuming a disturbance velocity of the form

$$\tilde{\mathbf{u}}(x, y, z, t) \equiv \mathbf{u}(y, t) \exp(i\alpha x + i\beta z),$$

with an analogous assumption for the disturbance pressure  $p$ , Eq. (1) becomes

$$\left[ \left( \frac{\partial}{\partial t} + i\alpha U - \frac{1}{R} \Delta \right) \Delta - i\alpha \frac{\partial^2 U}{\partial y^2} \right] \mathbf{v} = 0, \tag{2}$$

$$\left( \frac{\partial}{\partial t} + i\alpha U - \frac{1}{R} \Delta \right) \eta = -i\beta \frac{\partial U}{\partial y} \mathbf{v},$$

where the Laplacian takes the form  $\Delta = (\partial^2 / \partial y^2) - k^2$ , with  $k^2 = \alpha^2 + \beta^2$ . Setting  $\mathbf{v} = (v, \eta)^T$ , (2) can be written in matrix form<sup>4,6</sup>

$$\frac{d\mathbf{v}}{dt} = \Lambda \mathbf{v}, \quad \text{with} \quad \Lambda = \begin{bmatrix} \Omega & 0 \\ \Upsilon & \Sigma \end{bmatrix}. \tag{3}$$

The elements in the linearized dynamical operator  $\Lambda$  are

$$\Omega = \Delta^{-1} \left[ \left( -i\alpha U + \frac{1}{R} \Delta \right) \Delta + i\alpha \frac{\partial^2 U}{\partial y^2} \right],$$

$$\Upsilon = -i\beta \frac{\partial U}{\partial y},$$

$$\Sigma = -i\alpha U + \frac{1}{R} \Delta.$$

In the above form, for all cases of physical interest, i.e., whenever  $\alpha$  and  $\beta$  are not simultaneously zero, the operator  $\Lambda$  is not self-adjoint. This implies that the transient behavior of the system in Eq. (3) cannot be described by a single eigenmode.<sup>17,18</sup> Equation (3) retains its validity in the limit as  $t \rightarrow \infty$ , however, the asymptotic behavior of the system is obtained more efficiently using conventional eigenanalysis.

In the following, the inner product of two arbitrary complex vector quantities  $\mathbf{a}$  and  $\mathbf{b}$  is defined by

$$(\mathbf{a}, \mathbf{b}) = \int_\sigma \bar{\mathbf{a}}^T \cdot \mathbf{b} \, d\sigma,$$

where the over-bar denotes a complex conjugate and  $\sigma$  is the spatial extent of the domain. So defined, the inner product of a perturbation with itself is proportional to its kinetic energy. In the temporal analysis this is a function of time

$$E(t) = (\mathbf{u}, \mathbf{u}).$$

This measure represents a positive-definite quadratic form (norm) of physical significance. Scaling by the initial configuration's norm gives the disturbance's growth

$$G(t) = \frac{E(t)}{E(0)},$$

which quantifies the magnitude of a given perturbation as it evolves in time. In the context of the temporal approach outlined above, an optimal perturbation is an initial configuration of  $\mathbf{v}$  and  $\eta$  which maximizes growth at a specified time  $t = \tau$  and a given set of parameters,  $\alpha$ ,  $\beta$ ,  $R$ , and  $m$ .

The technique used here to determine the optimal initial configuration is based on the definition of the growth and the concept of the propagator. The propagator  $\Phi$  expresses the evolution of an initial solution from its conception through to a given time,  $t = \tau$

$$\mathbf{v}(\tau) = \Phi(\tau) \mathbf{v}(0).$$

Introducing  $\mathbf{A}$ , a rectangular transfer matrix between  $\mathbf{v}$  and  $\mathbf{u}$

$$\mathbf{u} = \mathbf{A} \mathbf{v}, \quad \text{with} \quad \mathbf{A} = \frac{1}{k^2} \begin{bmatrix} i\alpha (\partial / \partial y) & -i\beta \\ k^2 & 0 \\ i\beta (\partial / \partial y) & i\alpha \end{bmatrix},$$

it becomes possible to rewrite the expression for growth in terms of the initial solution and the propagator

$$G(\tau) = \frac{(\mathbf{A} \mathbf{v}(\tau), \mathbf{A} \mathbf{v}(\tau))}{(\mathbf{A} \mathbf{v}(0), \mathbf{A} \mathbf{v}(0))} = \frac{(\mathbf{A} \Phi(\tau) \mathbf{v}(0), \mathbf{A} \Phi(\tau) \mathbf{v}(0))}{(\mathbf{A} \mathbf{v}(0), \mathbf{A} \mathbf{v}(0))}.$$

An equivalent form of this expression is

$$G(\tau) = \frac{(\mathbf{v}(0), \Phi^*(\tau) \mathbf{A}^* \mathbf{A} \Phi(\tau) \mathbf{v}(0))}{(\mathbf{v}(0), \mathbf{A}^* \mathbf{A} \mathbf{v}(0))},$$

obtained by applying the definition of the adjoint in the energy norm, where the superscript  $*$  is used to indicate adjoint quantities. This is a Rayleigh quotient, and the growth will be maximized by the largest eigenvalue of the problem

$$(\mathbf{A}^* \mathbf{A})^{-1} \Phi^*(\tau) (\mathbf{A}^* \mathbf{A}) \Phi(\tau) \mathbf{v}(0) = G(\tau) \mathbf{v}(0).$$

The optimal initial configuration sought is the corresponding eigenvector. The linear operator multiplying the optimal on the left-hand-side is a positive-definite Hermitian form, consequently  $G(\tau)$  is real and positive, and the optimal perturbations are orthogonal to one another.

The simplest manner of obtaining the optimal perturbation is to apply power iterations of the form

$$\mathbf{v}(0)^{k+1} = (\mathbf{A}^* \mathbf{A})^{-1} \Phi^*(\tau) (\mathbf{A}^* \mathbf{A}) \Phi(\tau) \mathbf{v}(0)^k. \tag{4}$$

This process is equivalent to finding the largest singular value (norm) of the propagator; in this context the optimal perturbation is the propagator's largest singular vector. Two assumptions are inherent in the use of the power method: The first is that the initial guess for  $\mathbf{v}(0)$  is not orthogonal to the first singular vector, the second is that the singular values of the propagator are well-separated. Rapid convergence of the iterative procedure will be interpreted as an *a posteriori*

indication that these issues have been successfully addressed. The power method algorithm is broken into four distinct steps, working from right to left in Eq. (4)

1.  $\mathbf{v}(\tau)^k = \Phi(\tau)\mathbf{v}(0)^k$ ,
2.  $\mathbf{z}(\tau)^k = (\mathbf{A}^*\mathbf{A})\mathbf{v}(\tau)^k$ ,
3.  $\mathbf{z}(0)^k = \Phi^*(\tau)\mathbf{z}(\tau)^k$ ,
4.  $\mathbf{v}(0)^{k+1} = (\mathbf{A}^*\mathbf{A})^{-1}\mathbf{z}(0)^k$ .

Successive iterates can be scaled to ensure that their magnitudes remain reasonable.

As remarked by Luchini,<sup>12</sup> obtaining a matrix representation of the propagator  $\Phi$  is an involved undertaking, whereas the direct initial boundary value problem is known, and its adjoint can be readily found. The action of the propagators in steps 1 and 3 above can be replaced by integration of the direct and adjoint systems. Introducing the variable  $\tilde{\mathbf{a}} = (\tilde{a}, \tilde{b})^T$ , the adjoint system reads

$$\left[ \left( \frac{\partial}{\partial t} + U \frac{\partial}{\partial x} + \frac{1}{R} \Delta \right) \Delta + 2 \frac{\partial U}{\partial y} \frac{\partial^2}{\partial x \partial y} \right] \tilde{a} = - \frac{\partial U}{\partial y} \frac{\partial}{\partial z} \tilde{b},$$

$$\left( \frac{\partial}{\partial t} + U \frac{\partial}{\partial x} + \frac{1}{R} \Delta \right) \tilde{b} = 0. \tag{5}$$

The boundary conditions on  $\tilde{\mathbf{a}}$  are chosen in the process of integration by parts from which the system (5) is obtained. Here, these are set to be identical to those on  $\tilde{\mathbf{v}}$ . Note that this system's intrinsic direction of stable evolution is reversed, i.e., time flows backwards for this system, as indicated implicitly in step 3 above. Assuming periodicity in the stream- and span-wise directions as for the direct case results in an intermediate expression similar to Eq. (2). Casting Eq. (5) into matrix form analogous to Eq. (3) one obtains

$$\frac{d\mathbf{a}}{dt} = \Lambda^* \mathbf{a}, \quad \text{with} \quad \Lambda^* = \begin{bmatrix} \mathbf{\Omega}^* & \mathbf{Y}^* \\ 0 & \mathbf{\Sigma}^* \end{bmatrix}, \tag{6}$$

where the elements in the adjoint dynamical operator  $\Lambda^*$  are

$$\mathbf{\Omega}^* = \Delta^{-1} \left[ \left( -i\alpha U - \frac{1}{R} \Delta \right) \Delta - i2\alpha \frac{\partial U}{\partial y} \frac{\partial}{\partial y} \right],$$

$$\mathbf{Y}^* = -i\beta \Delta^{-1} \frac{\partial U}{\partial y},$$

$$\mathbf{\Sigma}^* = -i\alpha U - \frac{1}{R} \Delta.$$

The last relation in the adjoint system is a contribution from the time derivative terms

$$\int_0^\infty \frac{\partial}{\partial t} (\Delta \tilde{\mathbf{v}}^T \mathbf{a} + \tilde{\eta}^T \mathbf{b}) dy = \frac{\partial}{\partial t} [(\Delta \mathbf{v}, \mathbf{a}) + (\eta, \mathbf{b})] = 0,$$

and relates  $\mathbf{v}$  to  $\mathbf{a}$ . This expression implies that whatever conditions are chosen for the integration of Eqs. (3) and (6), the inner product given by

$$\epsilon = (\mathbf{B}\mathbf{v}, \mathbf{a}), \quad \text{with} \quad \mathbf{B} = \frac{1}{k^2} \begin{bmatrix} (\partial^2/\partial y^2) - k^2 & 0 \\ 0 & 1 \end{bmatrix},$$

remains constant in time. This requirement not only provides a link between the propagators  $\Phi$  and  $\Phi^*$  in Eq. (4) and a

practical implementation of the power iteration algorithm using the linearized dynamical operators in Eqs. (3) and (6), it also serves as a check on the accuracy of the method used for their integration.

Note that the kinetic energy of the perturbation can also be written as

$$E(t) = (\mathbf{B}\mathbf{v}, \mathbf{w}),$$

where  $\mathbf{w} = (-v, \eta)^T$ . The power iteration loop starts with an arbitrary guess for  $\mathbf{v}(0)$ , which after direct integration of (3) from  $t=0$  to  $t=\tau$  becomes  $\mathbf{v}^{(1)}(\tau)$ , characterized by a kinetic energy  $E^{(1)}(\tau)$ . Choosing  $\mathbf{a}^{(1)}(\tau) \equiv 1/k^2 \mathbf{w}^{(1)}(\tau)$  as a starting condition for (6),  $\epsilon^{(1)}$  is identified as the desired energy norm and must remain constant throughout the ‘‘backward-in-time’’ integration of the adjoint system from  $t=\tau$  to  $t=0$ . The initial conditions used for the direct equations at the start of the next loop are then  $\mathbf{v}^{(2)}(0) = -k^2 \mathbf{a}^{(1)}(0)$  and  $\eta^{(2)}(0) = k^2 \mathbf{b}^{(1)}(0)$ . This iterative procedure typically converges for the growth in five cycles or less.

### III. RESULTS

It remains to apply the procedures described above to a physical model. The numerical methods employed to obtain the results presented in this section comprise a Chebyshev collocation technique for the spatial discretization and implicit finite-differencing for temporal integration. Further details are given in the Appendix.

A self-similar boundary layer for the general case of nonzero pressure gradients is obtained when the external potential flow is assumed to vary proportionally to  $x^m$ , and no-slip conditions are imposed at the wall. The Falkner–Skan similarity solution for the nondimensional streamfunction  $f(\xi)$  corresponding to this situation is given by the nonlinear ordinary differential equation

$$f''' + \frac{m+1}{2} f'' f + m(1-f'^2) = 0,$$

where primes indicate derivatives with respect to the similarity variable

$$\xi = yx^{(m+1)/2},$$

and the boundary conditions are

$$f(0) = f'(0) = 0 \quad \text{and} \quad f(\xi \rightarrow \infty) \rightarrow 1.$$

The mean flow sought is described by  $U_e = x^m f'$ . Decelerated flow is described by  $-0.0904 < m < 0$ , where the lower limit corresponds to imminent separation, the Blasius boundary layer is recovered for  $m=0$ , whereas an accelerated flow is obtained for  $m > 0$ . Only classical solutions to the equations, characterized by monotonic increase of  $U$  with  $\xi$ , will be considered here. The Falkner–Skan profiles (and first derivatives) corresponding to the mean flows investigated here are shown in Fig. 1. Numerical values of the displacement thickness

$$\delta^* = \int_0^\infty (1-U) d\xi,$$

and the momentum thickness

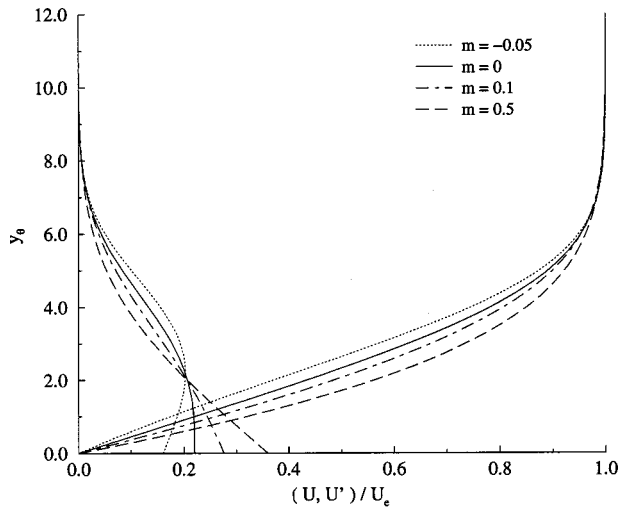


FIG. 1. Variation of the Falkner-Skan profile and its first derivative as a function of the imposed pressure gradient.

$$\theta = \int_0^\infty U(1-U)d\xi,$$

for the profiles shown, as well as the ratio of these two quantities, the shape factor  $H$ , are listed in Table I.

Optimal perturbations have been defined quite precisely in the previous section, it remains to describe the time frames over which they will be sought. Consider a perturbation described by the wave number pair  $(\alpha_0, \beta_0)$  in a mean flow parameterized by  $R$  and  $m$ . A *local* optimal is an initial configuration of  $v$  and  $\eta$  which excites the algebraic growth mechanism optimally at a given finite time  $t = \tau$ , the growth at this time is

TABLE I. Integral parameters for selected Falkner-Skan profiles.

$m$	$\delta^*$	$\theta$	$H$
-0.0904	3.446 04	0.867 979	3.970 19
-0.05	2.117 76	0.751 462	2.818 18
0	1.7208	0.664 115	2.591 11
0.1	1.347 87	0.556 593	2.421 64
0.5	0.854 69	0.3779	2.261 68
1	0.647 91	0.292 34	2.216 29

$$G = G(\alpha_0, \beta_0, \tau, R, m).$$

The *global* optimal disturbance for this set of parameters is the initial condition which maximizes the growth, i.e.,

$$\gamma = \max_{\forall t} G(\alpha_0, \beta_0, R, m),$$

its specification is completed by  $t_\gamma$ , the time at which this growth occurs. Generally, local optima are sought for times smaller than  $t_\gamma$ . The largest global growth obtained for any set of wave numbers

$$\Gamma = \max_{\forall \alpha, \beta} \gamma(R, m),$$

is a characteristic only of the base flow.

This study's principal objective is to quantify the magnitude of the maximum global growth  $\Gamma$ , and to determine the physical characteristics of the disturbance responsible for it. Since a linear mechanism is responsible for algebraic growth, it is reasonable to expect  $t_\gamma$  to scale linearly, and in light of the boundary layer nature of the flow, quadratic scal-

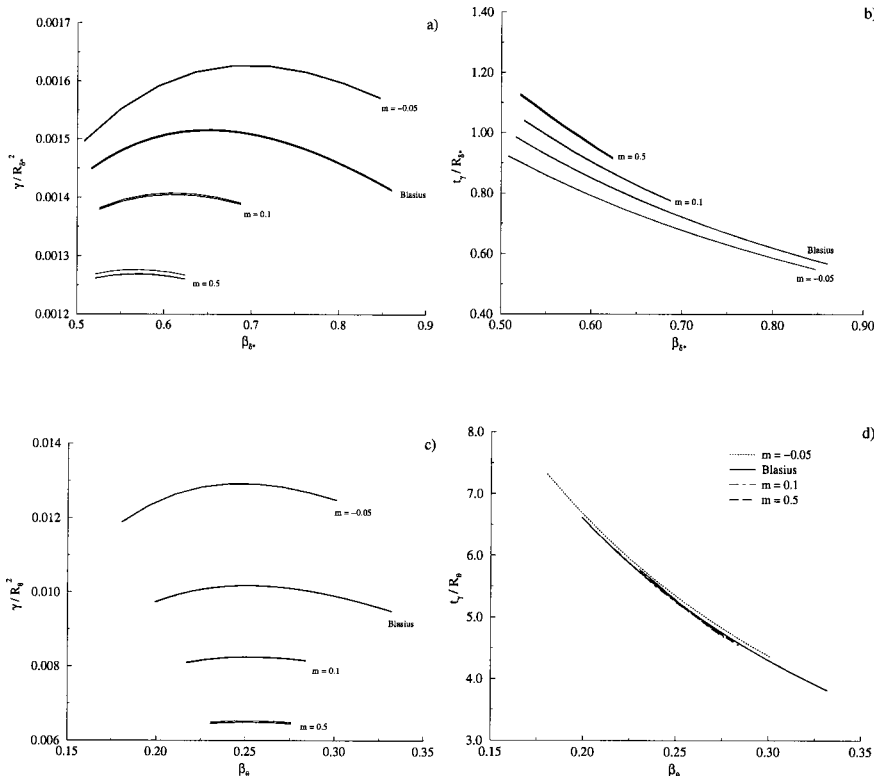


FIG. 2. Variation of the maximum global growth, scaled by  $R^2$ , and its characteristic development time, scaled by  $R$ , shown as a function of the span-wise wave number. Parts (a) and (b) use the displacement thickness, parts (c) and (d) use the momentum thickness.

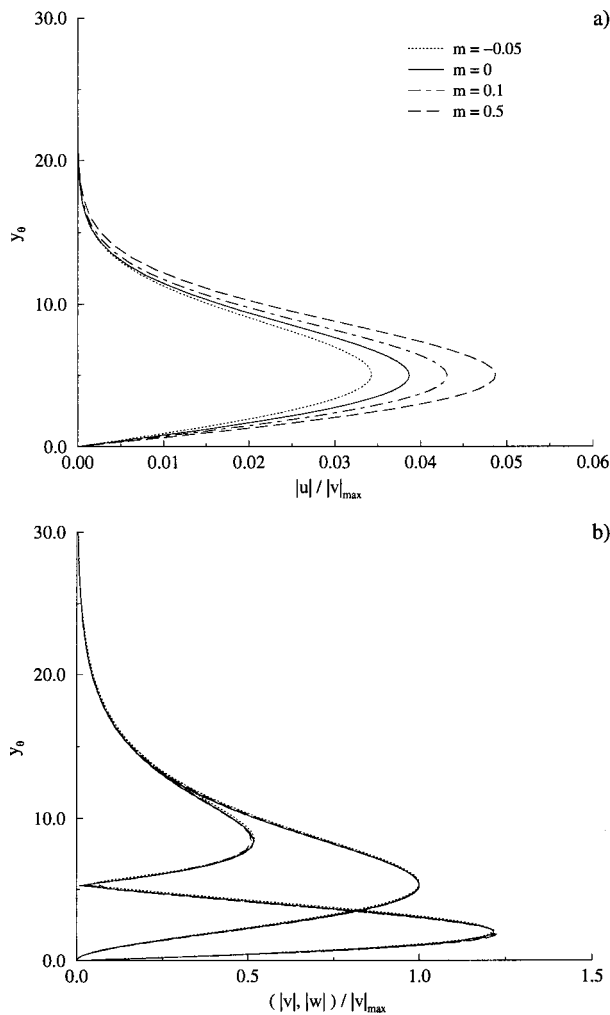


FIG. 3. (a) The effect of pressure gradient on the initial stream-wise perturbation velocity for maximum global optimal, scaled by  $|v|_{\max}$ . ( $R_\theta=166$ ) (b) Initial normal and span-wise velocity profiles for the same conditions, similarly scaled.

ing of  $\Gamma$  with the Reynolds number can be anticipated. On the other hand, its behavior with respect to variations in  $m$  cannot be foreseen.

Results for the Blasius boundary layer have shown that flow structures infinitely elongated in the stream-wise sense experience the most amplification. It was found that this is also the case in boundary layers described by the Falkner-Skan profiles. In order to determine the scaling behavior of maximum global optimal perturbation it is necessary to evaluate  $\gamma$  and  $t_\gamma$  over the range of  $\beta$  where the maximum is anticipated at different Reynolds numbers and pressure gradients.

TABLE II. Variation in the characteristics of maximum global optimals with pressure gradient ( $R_\theta=166$ ).

$m$	$\beta_\theta$	$\Gamma$	$t_\Gamma$
-0.05	0.247 05	356.4	898.2
0	0.251 14	280.7	870.8
0.1	0.252 23	227.4	863.5
0.5	0.251 44	179.1	869.7

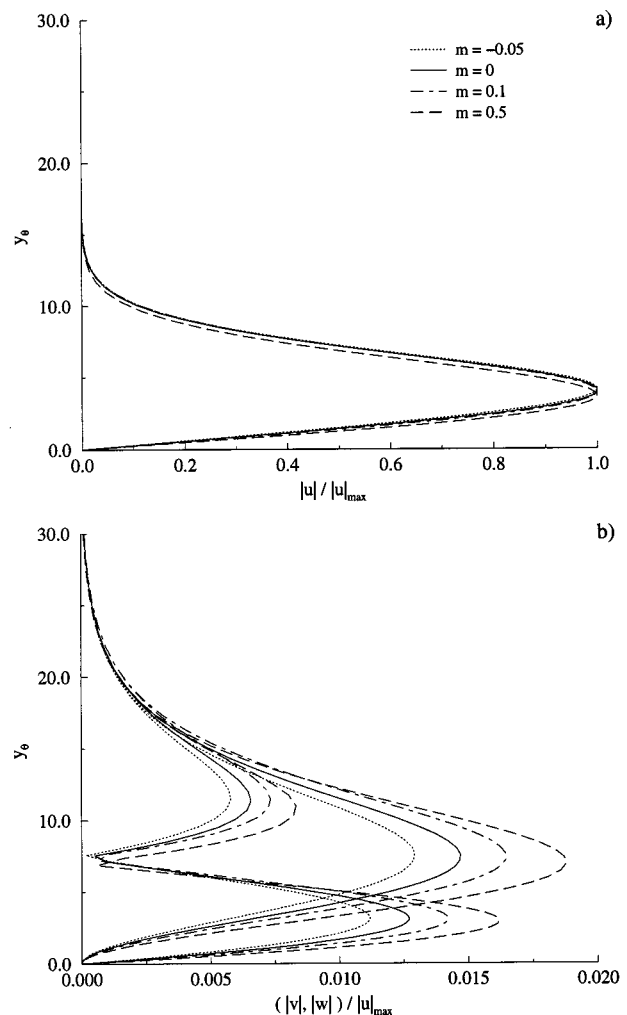


FIG. 4. (a) Stream-wise perturbation velocity magnitude profiles at  $t_\Gamma$ , scaled by  $|u|_{\max}$ . (b) Normal and span-wise velocity magnitudes at  $t_\Gamma$ .

Figure 2 shows  $\gamma$  and  $t_\gamma$  at the four values of  $m$  indicated. For each imposed pressure gradient, results corresponding to three arbitrary Reynolds numbers are shown. Figures 2(a) and 2(b) show the results of scaling with respect to  $R_{\delta^*}$ , the Reynolds number defined by the displacement thickness, and Figs. 2(c) and 2(d) show what happens when scaling with  $R_\theta$ , the Reynolds number defined with the momentum thickness. Figures 2(a) and 2(c) confirm the expected quadratic scaling of the growth with Reynolds number, Figs. 2(b) and 2(d) show  $t_\gamma$  scales linearly. Either scaling accounts well for differences in Reynolds number, and the effect of pressure gradient is made immediately evi-

TABLE III. Variation in the characteristics of maximum global optimals with Reynolds number (Blasius boundary layer).

$R_\theta$	$\beta_\theta$	$\Gamma$	$t_\Gamma$
166.0	0.251 15	280.7	870.8
385.9	0.251 19	1515.1	2023.4
498.1	0.251 30	2523.7	2610.2
	Butler & Farrell (Ref. 4)		
385.9	0.25	1514	2016

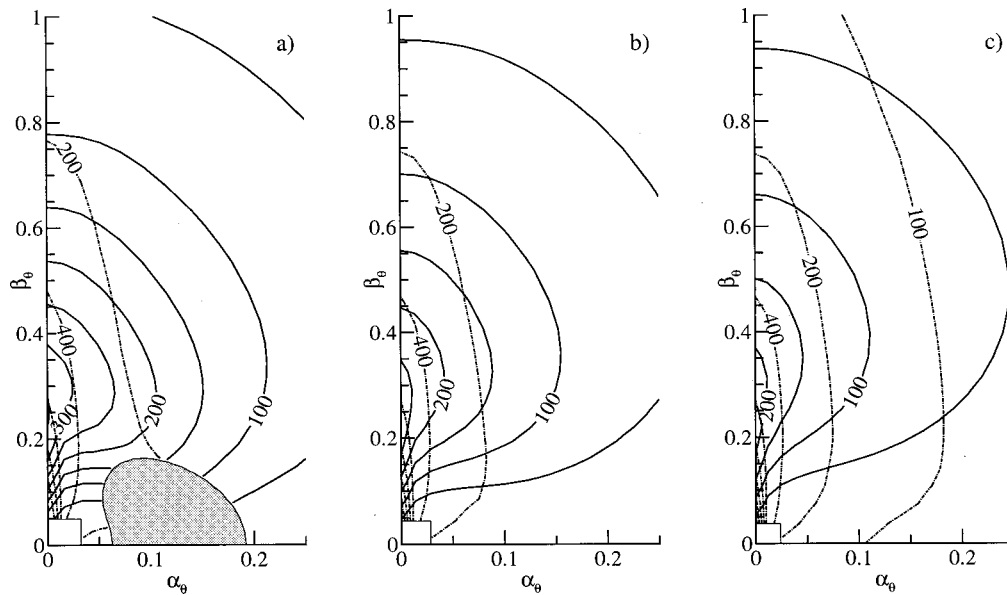


FIG. 5. Contours of  $\gamma$  (solid lines) and  $t_\gamma$  (dot-dash lines) in the wave number plane for  $R_\theta=166$ . (a)  $m=-0.05$ , disturbances in the shaded region are exponentially unstable. (b) Blasius. (c)  $m=0.1$ . In all cases, the increment between level curves of  $t_\gamma$  towards the origin is 400. Note the 4:1 axis ratio.

dent. The results show that, in comparison to the Blasius boundary layer, optimal perturbations in flows subject to adverse pressure gradients experience greater amplification, and those in accelerated flows enjoy less amplification.

Notable is that, when scaled with  $\theta$ , the span-wise wave number for  $\Gamma$  appears to be independent of the mean flow conditions,  $\beta_\theta \approx 1/4$ . Even more remarkable is how well  $\theta$  scaling accounts for the variation in  $t_\gamma$  resulting from differences in the base flow. A similar result for the neutral curve of Görtler vortices is well-established.<sup>19</sup> Since momentum thickness scaling appears to reveal some universal behavior in the algebraic growth mechanism, it will be used to report all results which follow. Aside from time, those quantities for which this has implications are indicated by a subscript “ $\theta$ .”

Tables II and III present some numerical results. The former shows how the characteristics of the  $\Gamma$  point vary with changes in  $m$  ( $R_\theta$  is kept constant), and the latter shows how these characteristics vary with changes in Reynolds number at a given pressure gradient. In this case the Blasius boundary layer has been chosen, so the results can be compared with those of Butler and Farrell. The agreement is remarkably good, the slight variation between them might stem from the different spatial discretization, or to the approximation used for the continuous spectrum.

From the engineering point of view, a perturbation is of most interest at its conception. The velocity profiles of the optimal perturbations reported in Table II are shown in Fig. 3 (the effect of varying  $m$  is sought since the Reynolds scaling can be inferred directly). In each case,  $\mathbf{u}$  has been scaled such that  $|\mathbf{v}(0)|_{\max} \equiv 1$ , the maximum normal velocity component is unity. Unsurprisingly, the optimal is seen to be a stream-wise oriented vortex situated mainly within the boundary layer, but extending some distance into the free-stream. When scaled with the momentum thickness, the shape of the starting vortex is independent of the imposed

pressure gradient. The magnitude of the initial stream-wise velocity component varies in proportion to  $m$ , but is in all cases two orders of magnitude less than the cross-flow components.

In order to answer the second question motivating this work, Fig. 4 shows the evolved state of the optimal perturbations at  $t=t_\Gamma$ . Here,  $\mathbf{u}$  has been scaled by the maximum stream-wise velocity component,  $|u(t_\Gamma)|_{\max} \equiv 1$ . The resemblance in shape, despite the different external flow conditions, for the stream-wise velocity components is remarkable. Note that for  $\alpha=0$  the system in Eq. (2) simplifies significantly, and the effect of the mean flow is felt only

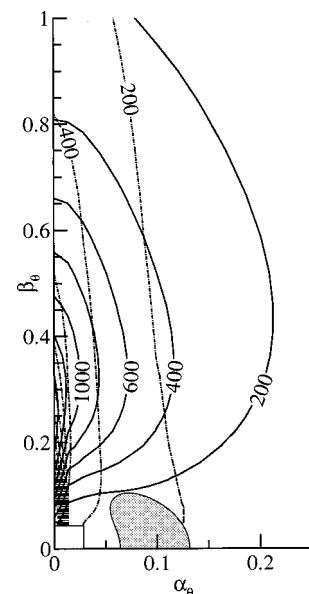


FIG. 6. Contours of  $\gamma$  (solid lines) and  $t_\gamma$  (dot-dash lines) in the wave number plane for Blasius flow at  $R_\theta=386$ . The exponentially unstable area for this flow is shaded.

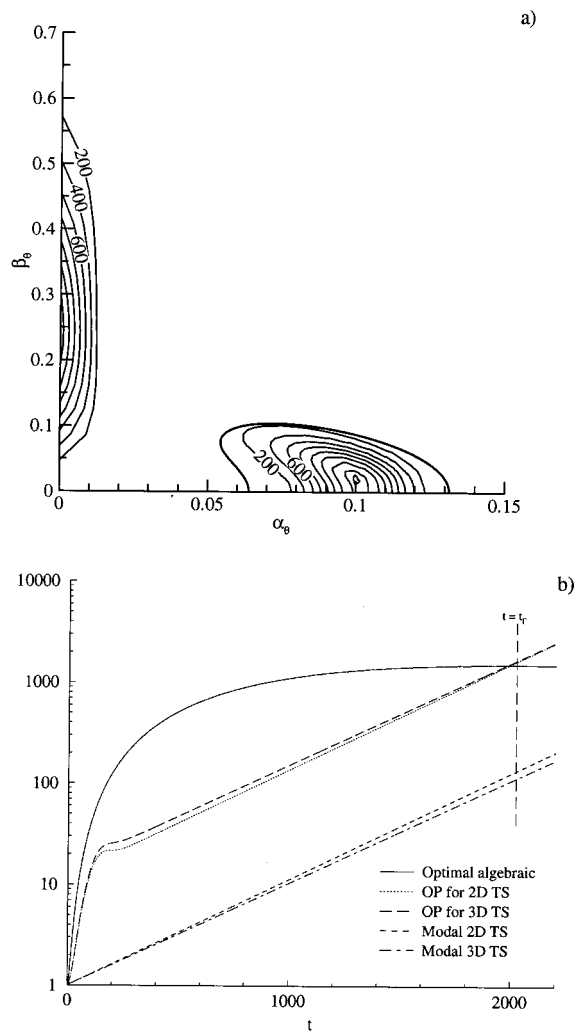


FIG. 7. (a) Contours of  $G(t_\Gamma)$  for  $R=386$  (local optimum growth). The critical stability limit is indicated by the thick line. The innermost level curve in the exponentially unstable area is  $G=1660$ . (b) Growth amongst the various mechanisms.

through its first derivative in the source term for the  $\eta$  equation (cf. Fig. 1). The remnants of the initial vortex are still present although it has diffused outwards away from the wall. The final state of the optimal perturbation for the algebraic instability strongly resembles the streaks frequently observed in boundary layers. This finding is in good agreement with the spatial results reported in Refs. 5 and 12.

To this point, it might be said that only worst-case scenarios have been considered, since incoming disturbances are unlikely to be configured to optimally excite the maximum global growth. The pervasiveness of transient growth in a boundary layer for a wide range of wave number combinations is apprehended immediately from a plot of level curves of  $\gamma$  (and  $t_\gamma$ ) in the wave number plane. The series of plots presented in Fig. 5 shows such isolines for  $m = -0.05, 0, 0.1$ , in order to make the effect of pressure gradient immediately evident. For all cases, significant algebraic growth occurs in a large part of the wave number plane examined. The first part of the figure corresponds to  $m = -0.05$ , for which a section of the wave number plane experiences exponential instability. This section has been

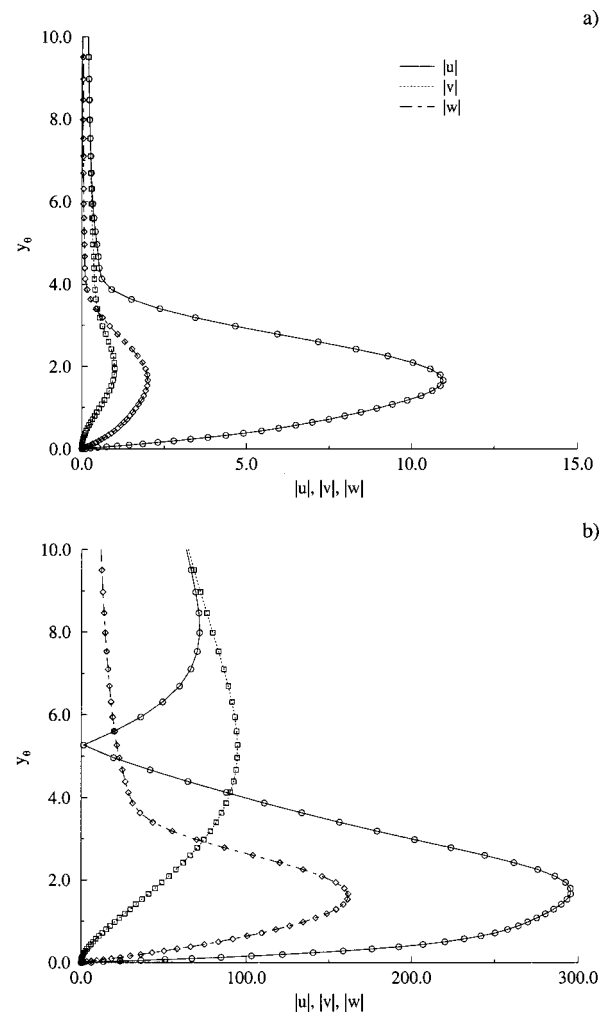


FIG. 8. (a) Optimal initial excitation for the three-dimensional Tollmien-Schlichting mode exhibiting greatest transient growth over time  $t=t_\Gamma$ . The symbols show the eigenfunction of the adjoint stability problem. (b) The optimally excited three-dimensional Tollmien-Schlichting mode at  $t_\Gamma$ . The symbols denote the mode shape predicted by linear stability theory.

shaded. The figures are otherwise similar, with growth decreasing radially away from the  $\Gamma$  point. For each given  $\alpha_\theta$  ( $\alpha_\theta > 0$ ), most growth occurs for perturbations characterized by weakly increasing values of  $\beta_\theta$ , with  $\beta_\theta \approx 1/3$ . As might be inferred from Fig. 2, greater growth is experienced for adverse pressure gradients, whereas growth is damped for favorable pressure gradients.

Figure 6, which shows  $\gamma$  for a Blasius boundary layer at  $R_\theta = 385.9$ , is included to show the effect of increasing Reynolds number, an effect apparently not dissimilar to imposing an adverse pressure gradient. The shaded region again indicates exponential growth. Remark that for all cases  $t_\gamma$ ,

TABLE IV. Modes of largest asymptotic two dimensional and most transiently amplified three-dimensional Tollmien-Schlichting waves for  $t=t_\Gamma$ .

$\alpha_\theta$	$\beta_\theta$	$\Re(\omega_\theta)$	$\Im(\omega_\theta)$	$G(t_\Gamma)$
0.1030	0	$3.651 \times 10^{-2}$	$1.213 \times 10^{-3}$	1636.3
0.1030	0.0190	$3.705 \times 10^{-2}$	$1.171 \times 10^{-3}$	1678.0

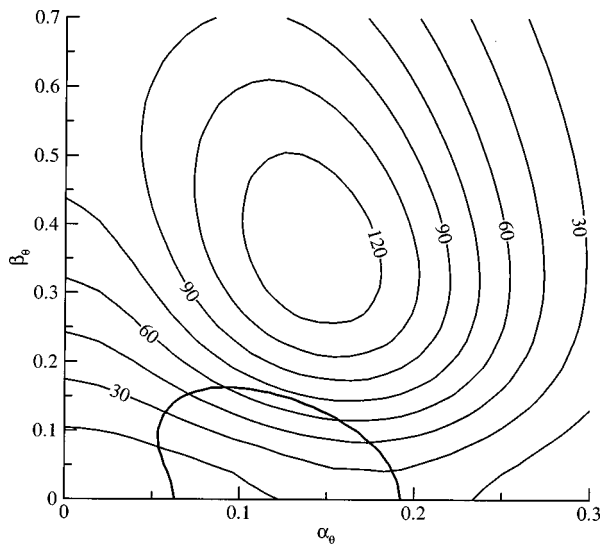


FIG. 9. Contours of  $G(t \approx 100)$  for  $R_\theta = 221$ ,  $m = -0.05$ . The critical stability limit is indicated by the thick line.

while generally moderate, experiences a sharp peak for long wave-length perturbations, and  $t_\Gamma$  lies just at the edge of this peak. As evidenced by the increase in  $t_\gamma$  towards the origin of the wave number plane, long wave-length disturbances evolve very slowly, and the parallel flow assumption fails. In light of this, data has not been collected in this area, as indicated by the blanked-out region in Figs. 5 and 6.

It is interesting to assess the maximum global optimal's relative strength by comparing it to local optima for  $t_\Gamma$ . This is of particular interest for Reynolds numbers above critical, since it will show whether the algebraic growth mechanism can successfully compete with the Tollmien–Schlichting instability. Contours of  $G(t_\Gamma)$  for the Blasius boundary layer at  $R_\theta = 385.9$  are shown in the first part of Fig. 7. Evidently, stream-wise oriented vortices of various wave-lengths exhibit strong growth, but substantial local growth also occurs in the linearly unstable region, where for these conditions an oblique Tollmien–Schlichting wave obtains the largest response. (While growth is unbounded as time becomes large in this region, it is bounded and well-defined for finite time.) The results show that over a finite period algebraic growth is fully capable of competition with Tollmien–Schlichting waves. Furthermore, perturbations with wave numbers in the vicinity of either mechanism will experience growth.

The situation is considered in more detail in the second part of Fig. 7, which plots the growth exhibited by the various competing disturbances. The two lower curves correspond to growth rates obtained from linear stability theory, reported in Table IV. In this context it is assumed that the corresponding Tollmien–Schlichting wave exists in the boundary layer at  $t=0$  and develops exponentially. The slightly lesser growth rate corresponds to the oblique wave which experiences the most amplification at  $t_\Gamma$ , the other corresponds to the most amplified Tollmien–Schlichting wave (two-dimensional in accordance with Squire's theorem). The other three curves correspond to optimally perturbed mechanisms. The solid line is the growth obtained by the stream-wise vortex, whereas the dashed and dotted lines

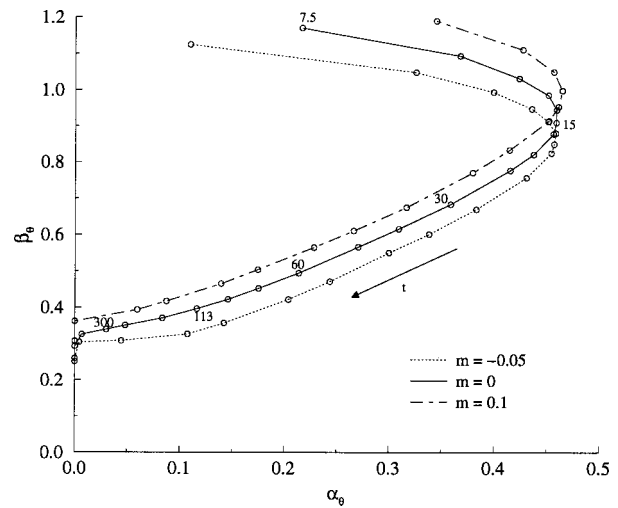


FIG. 10. Effect of pressure gradient on the evolution of the wave number of the maximum local optimum with time. Sampled at times before  $t_\Gamma$  for  $R_\theta = 166$ ;  $t$  indicated for  $m=0$ .

show the growth obtained by the optimally perturbed Tollmien–Schlichting (TS) waves. The greater growth of the oblique wave is due to its larger transient amplification. At conception and shortly afterwards, the algebraic mechanism's growth is approximately an order of magnitude larger than its nearest competitor. Optimally perturbed TS waves attain an asymptotic state relatively quickly, further growth is at the rate predicted by classical theory.

The optimal configuration for exciting the oblique TS wave is shown in Fig. 8. Hill's study of TS receptivity<sup>20</sup> demonstrated that these waves are most receptive to disturbances given by the eigenfunctions of the adjoint Orr–Sommerfeld equations. The symbols superposed on the profiles correspond to these eigenfunctions. At  $t=t_\Gamma$  this perturbation has evolved into the state depicted in the second part of Fig. 8, the modal state predicted by classical stability theory is represented by the superposed symbols.

Should the above results be transferable to the spatial context via some transform based upon an  $\mathcal{O}(1)$  convection speed, it follows from the long evolution period for global optimals that a substantial stream-wise development distance of  $\mathcal{O}(R\delta)$  is necessary for the streak to emerge. This is borne out by the Reynolds number scaling of  $t_\gamma$  in Fig. 2, rendering the validity of the parallel flow hypothesis rather questionable. Also, it seems improbable that a (maximum) global optimal perturbation can develop undisturbed over such a long period in an actual flow. These arguments make it natural to inquire about the behavior of local optimals in the short-time limit.

As a first step in this direction, consider the competition between TS waves and the algebraic mechanism for adverse pressure gradients. The maximum global optimal takes so long to develop in decelerated flows that the TS mechanism attains growth two orders of magnitude larger over the same period. The situation at short time is completely different as shown clearly in Fig. 9, which presents level curves of  $G$  at  $t=99.8$ . The limit of exponential amplification is indicated by a thick line. Optimals on a significant portion of the wave

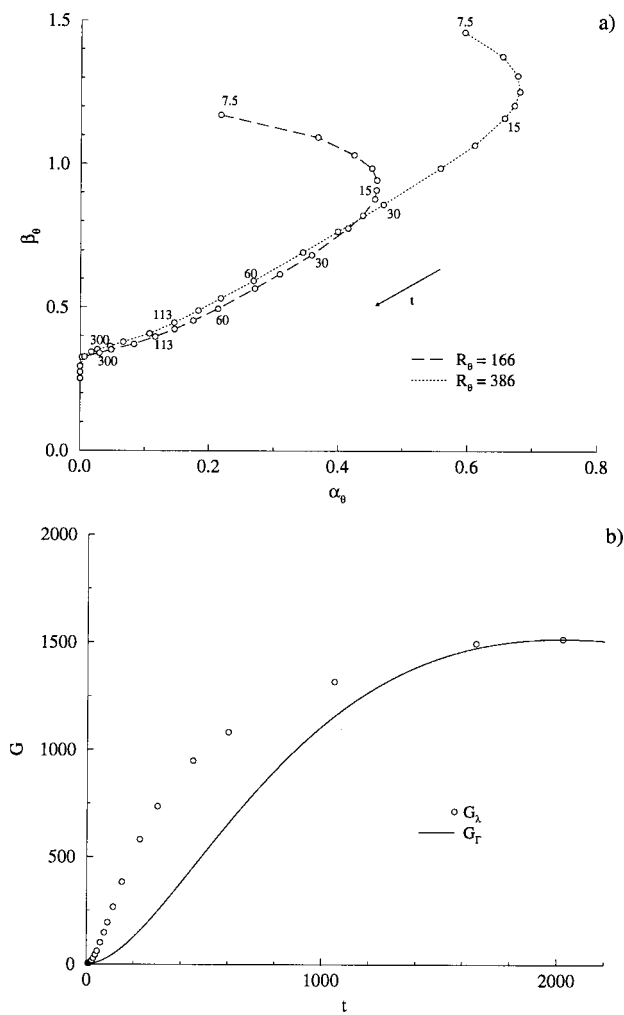


FIG. 11. (a) The effect of Reynolds number on the evolution of the wave number of the maximum local optimum, shown for Blasius flow. (b) Comparison between local and global optimal growth for  $R_\theta = 386$ .

number plane enjoy two orders of magnitude growth. Interestingly, this growth occurs for oblique structures. In contrast, over this short time the (optimally excited) TS mechanism has yet to manifest itself.

It turns out that maximum local optima tend to be oblique, as shown by Figs. 10 and 11. These depict the wave number pair of the local optimal experiencing maximum amplification sampled for times between inception and  $t_T$  (the target time is indicated for reference). Figure 10 shows how pressure gradient affects this behavior,  $R_\theta = 166$  has been fixed and  $m$  is allowed to vary. It can be seen from Fig. 11 that change in the Reynolds number has a much larger effect, particularly at very short times. The second part of Fig. 11 compares the growth obtained by local optima to that experienced by the maximum global optimal. Oblique local optima attain greater growth than the global optimal over shorter periods by efficiently extracting energy from the mean flow via the Orr mechanism.<sup>21,22</sup>

Oblique local optimal perturbations, with stream- and span-wise wave-lengths of comparable magnitude, cannot be determined by a theory based upon boundary layer scalings, but in light of the large growth they can provoke, they should

clearly not be dismissed. While the stream-wise oriented vortex may be the most effective streak generator, it is not alone: The oblique local optima also develop into disturbances where the stream-wise component plays a predominant rôle.

#### IV. CONCLUDING REMARKS

Initial configurations of perturbation normal velocity and vorticity which obtain the greatest response for a given input have been studied for the Falkner–Skan boundary layer. Conditions corresponding to adverse, zero and favorable pressure gradients are considered using a direct–adjoint technique in the temporal framework. This technique depends neither upon the eigenvectors of the generalized linear stability eigenproblem nor upon the choice of an arbitrary set of basis functions to discretize the propagator. This permits the boundary layer problem on the half-plane to be attacked directly, by-passing issues concerning the discretization of the continuous spectrum characteristic of such problems.

The disturbance which evokes the greatest response over all time is a stream-wise oriented vortex which gives rise to a stream-wise streak. The response is quantified by its growth, defined as the ratio of final to initial perturbation kinetic energies. For a given pressure gradient, the time in which such growth is attained is found to scale linearly, and the growth itself quadratically, with the Reynolds number. The effect of adverse pressure gradient is to enhance growth, whereas a favorable pressure gradient at the same Reynolds number has a damping effect. The maximal growth and its characteristic development time are found to scale best with the nondimensional boundary layer momentum thickness. Similarly scaled, the perturbation velocity profiles are remarkably similar.

In the case of the Blasius boundary layer, the results obtained are in excellent agreement with previous work using the temporal framework by Butler and Farrell.<sup>4</sup> Furthermore, the optimal’s general characteristics agree favorably with those found by Luchini<sup>12</sup> and Andersson *et al.*<sup>5</sup> using spatial analysis. Those findings showed good agreement between the final state and experimentally observed perturbation velocity profiles.

Initial configurations which maximize growth at a set time shorter than that required for maximal possible excitation, termed local optima in this work, have shown the capacity for significant amplification. Such perturbations are shown to be oblique for periods up to about a third of the characteristic time required for maximum growth, and evolve downstream into streaks.

The current method’s applicability to receptivity studies is straightforward. It is demonstrated in a quantitative fashion that the optimally stimulated algebraic growth mechanism is capable of competing with Tollmien–Schlichting waves in Blasius flow, even when these are also optimally excited. Algebraic growth is dominant at short times for all flow conditions considered.

It is apparent that even within the restrictions of the parallel flow temporal framework much can be learned about the transient behavior of boundary layers subject to pressure

gradients. Current work focuses on the search for local and global spatial optimals, in three-dimensional boundary layers.

## ACKNOWLEDGMENTS

The authors are pleased to acknowledge extensive discussions with Paolo Luchini on the subjects of algebraic growth and adjoint methods. Paul Andersson, Mejdí Azaïez, and Spyros Gavrilakis were generous with their time and advice. PC was supported by Swiss National Science Foundation Grant No. 2100-52'592.97.

## APPENDIX: NUMERICAL IMPLEMENTATION

All calculations were carried out in double precision on an engineering work-station using the Matlab linear algebra package.<sup>23</sup>

Equations (3) and (6) are discretized using the method of lines: Chebyshev collocation is used for the spatial discretization and a second-order backward Euler finite-difference scheme is used in the temporal discretization.

The unknowns are represented at collocation points given by the Chebyshev–Gauß–Lobatto nodes, and derivatives are obtained by matrix-vector multiplication with the differentiation matrix. The DMSuite routines by Weideman and Reddy<sup>24</sup> are used to obtain the Chebyshev–Gauß–Lobatto collocation points and the Chebyshev differentiation matrices. This package has been designed to circumvent error arising from finite-precision arithmetic. Boundary conditions are imposed by replacing rows in the original operator matrices. This renders the inverse Laplacian appearing in  $\Omega$  and  $\Omega^*$  well-posed. An algebraic stretching is used to transform the computational domain into the physical one,  $0 \leq y \leq y_\infty$

$$y_j = \frac{y_\infty H}{2} \frac{1 + x_j}{1 + H - x_j},$$

where  $H$  is a constant stretching factor. Integral quantities, such as the inner product, can be obtained efficiently using Gaussian quadrature rules adjusted by the Jacobian of the mapping given above.

The temporal integration requires a fairly accurate, reliable and efficient method. A second-order backward Euler discretization of Eqs. (3) and (6) is used. Time advancement involves matrix-vector multiplication, and storage for two previous solutions is required.

Numerical parameters were determined by grid convergence study. A stretching factor of  $H=1/9$  was used, which places half the points inside the boundary layer, and the outer boundary has been fixed at  $y_\infty \geq 80$ . All data was obtained using  $n \geq 84$  collocation points and  $\delta t \leq 0.2$ .

A line search algorithm based on golden section search and parabolic interpolation was employed to determine  $t_\gamma$  for global optimals. Searches involving two parameters, i.e., those for maximum global and local optimal perturbations, were performed using a simplex search method.

Finally, note that the generalized eigenvalue problem arising in classical stability theory is easily obtained from Eq. (3). The solution's behavior in time is assumed to go as

$$\mathbf{v}(y,t) = \hat{\mathbf{v}}(y) \exp(-i\omega t),$$

where the circular frequency is complex. Equation (3) becomes simply

$$-i\omega \hat{\mathbf{v}} = \Lambda \hat{\mathbf{v}}, \quad (\text{A1})$$

which is efficiently inverted using the QZ algorithm. Modal results presented here have been obtained using this technique.

<sup>1</sup>T. Ellingsen and E. Palm, "Stability of linear flow," *Phys. Fluids* **18**(4), 487 (1975).

<sup>2</sup>M. T. Landahl, "A note on an algebraic instability of inviscid parallel shear flows," *J. Fluid Mech.* **98**, 243 (1980).

<sup>3</sup>P. Luchini, "Reynolds-number independent instability of the boundary layer over a flat surface," *J. Fluid Mech.* **327**, 101 (1996).

<sup>4</sup>K. M. Butler and B. F. Farrell, "Three-dimensional optimal perturbations in viscous shear flow," *Phys. Fluids A* **4**(8), 1637 (1992).

<sup>5</sup>P. Andersson, M. Berggren, and D. S. Henningson, "Optimal disturbances and bypass transition in boundary layers," *Phys. Fluids* **11**(1), 134 (1999).

<sup>6</sup>S. C. Reddy and D. S. Henningson, "Energy growth in viscous channel flows," *J. Fluid Mech.* **252**, 209 (1993).

<sup>7</sup>W. O. Criminale, T. L. Jackson, D. G. Lasseigne, and R. D. Joslin, "Perturbation dynamics in viscous channel flows," *J. Fluid Mech.* **339**, 55 (1997).

<sup>8</sup>L. H. Gustavsson, "Energy growth of three-dimensional disturbances in plane Poiseuille flow," *J. Fluid Mech.* **224**, 241 (1991).

<sup>9</sup>L. M. Mack, "A numerical study of the temporal eigenvalue spectrum of the Blasius boundary layer," *J. Fluid Mech.* **73**, 497 (1976).

<sup>10</sup>D. G. Lasseigne, R. D. Joslin, T. L. Jackson, and W. O. Criminale, "The transient period for boundary layer disturbances," *J. Fluid Mech.* **381**, 89 (1999).

<sup>11</sup>J.-F. Laccarra and O. Talagrand, "Short-range evolution of small perturbations in a barotropic model," *Tellus, Ser. A* **40**(2), 81 (1988).

<sup>12</sup>P. Luchini, "Reynolds-number independent instability of the boundary layer over a flat surface, Part 2: Optimal perturbations," *J. Fluid Mech.* (in press).

<sup>13</sup>P. Luchini and A. Bottaro, "Görtler vortices: a backward-in-time approach to the receptivity problem," *J. Fluid Mech.* **363**, 1 (1998).

<sup>14</sup>P. J. Schmid, S. C. Reddy, and D. S. Henningson, "Transition thresholds in boundary layer and channel flows," in *Advances in Turbulence VI* (Kluwer Academic, 1996), pp. 101–104.

<sup>15</sup>S. C. Reddy, P. J. Schmid, J. S. Baggett, and D. S. Henningson, "On stability of streamwise streaks and transition thresholds in plane channel flows," *J. Fluid Mech.* **365**, 269 (1998).

<sup>16</sup>*Turbulence and Transition Modelling*, edited by M. Hallböck, D. S. Henningson, A. V. Johansson, and P. H. Alfredsson (Kluwer Academic, Dordrecht, 1996); Lecture notes from the ERCOFTAC/IUTAM summer school held in Stockholm, 12–20 June, 1995.

<sup>17</sup>L. N. Trefethen, "Pseudospectra of linear operators," in *ICIAM '95: Proceedings of the Third International Congress on Industrial and Applied Mathematics*, edited by Klaus Kirchgässner, Oskar Mahrenholtz, and Reinhard Mennicken (Akademie-Verlag, 1996).

<sup>18</sup>B. F. Farrell and P. J. Ioannou, "Generalized stability theory, Part I: Autonomous operators," *J. Atmos. Sci.* **53**(14), 2025 (1996).

<sup>19</sup>*Laminar boundary layers*, edited by L. Rosenhead (Oxford University Press, Oxford, 1963).

<sup>20</sup>D. C. Hill, "Adjoint systems and their role in the receptivity problem for boundary layers," *J. Fluid Mech.* **292**, 183 (1995).

<sup>21</sup>B. F. Farrell, "Optimal excitation of perturbations in viscous shear flow," *Phys. Fluids* **31**(8), 2093 (1988).

<sup>22</sup>B. F. Farrell and P. J. Ioannou, "Optimal excitation of three-dimensional perturbations in viscous constant shear flow," *Phys. Fluids A* **5**(6), 1390 (1993).

<sup>23</sup>The MathWorks, Natick, MA, *Using MATLAB version 5*, revised for MATLAB 5.1 edition, June 1997.

<sup>24</sup>J. A. C. Weideman and S. C. Reddy, A MATLAB differentiation matrix suite. Available at <http://osu.orst.edu/~weidemaj/differ.html>, August 1998.